



Numerical Simulation on the Interaction Modes Between Hydraulic and Natural Fractures Based on a New SPH Method

Yu Shuyang¹ · Ren Xuhua¹ · Wang Haijun² · Zhang Jixun¹ · Sun Zhaohua³

Received: 31 January 2021 / Accepted: 11 April 2021 / Published online: 3 May 2021
© King Fahd University of Petroleum & Minerals 2021

Abstract

In order to study the interaction mechanisms between hydraulic fractures (HF) and natural fractures (NF), a new numerical method named 2P-IKSPH has been proposed. The interactions between HF and NF under different conditions are simulated, results show that under the condition of low vertical confining pressure and low injecting rate, NF initiates at one tip closer to the horizontal boundary; under the condition of high vertical confining pressure, high injecting rate and small inclination angle of NF, the branching phenomenon occurs. The confining pressure, inclination angle and injecting rate all have significant impacts on the characteristic loads (e.g., HF initiation pressure, approaching pressure and NF initiation pressure). The research results can provide some references for the understanding of interaction mechanisms between HF and NF; meanwhile, developing high performance 3D 2P-IKSPH program will be the future research directions.

Keywords 2P-IKSPH · Hydraulic fracturing · Natural fractures · Interaction modes · Numerical simulation

1 Introduction

Shale gas is mainly stored in shale in the form of adsorption or free state, but the porosity and permeability of shale are very low, which brings great difficulties and challenges to its mining efficiency [1–4]. Hydraulic fracturing technology, as an effective means to increase crack opening, has been introduced into the field of oil exploitation since 1949 [5]. Subsequently, it has been widely used in shale gas mining [6] and extraction of water from hard crystalline rock [7]. Meanwhile, hydraulic fracturing technique is also widely used in measuring rock mass in situ stress [8]. However, large amounts of natural fractures exist in the rock masses, as shown in Fig. 1 [9]. Complex joints help to form complex fracture networks, which increase the hydraulic fracturing area. Therefore, the understandings of the interaction laws

between HF and NF will undoubtedly play an important role in promoting shale gas exploitation.

Interactions between NF and HF pose more challenges in the fracturing design and its execution [10]. Previous studies on the interactions between HF and NF mainly focus on the experiments, theory and numerical simulations. Experimental investigations are the most direct way to explore the interaction laws of NF and HF [11–13]. However, experimental studies have the disadvantages of long time period, high expense and discrete results; at the same time, its internal mechanisms cannot be directly expressed. Based on the experimental results, many scholars tried to express the theory of HF and NF interactions [14–16]. Nevertheless, theoretical model can only solve some relatively simple conditions, and complex fracture networks will lead to extremely complex mathematical expressions. As the ‘third method’ of scientific research [17], numerical simulation can not only verify the theoretical analytical solutions and experimental results, but also clarify the hydraulic fracturing mechanisms. Therefore, many numerical methods have been developed and applied to the simulations of interactions of HF and NF. Finite element method (FEM) has been one of the earliest methods to study hydraulic fracturing; however, the propagation, fusion and penetration of cracks need to change the mesh grids at every time step, so the applications are

✉ Ren Xuhua
yushuyang_hhu@163.com

¹ College of Water Conservancy and Hydropower, Hohai University, Nanjing 210098, China

² State Key Laboratory of Hydrology-Water Resource and Hydraulic Engineering, Nanjing Hydraulic Research Institute, Nanjing 210029, China

³ School of Transportation and Civil Engineering, Nantong University, 9 Seyuan Road, Nantong 226019, China



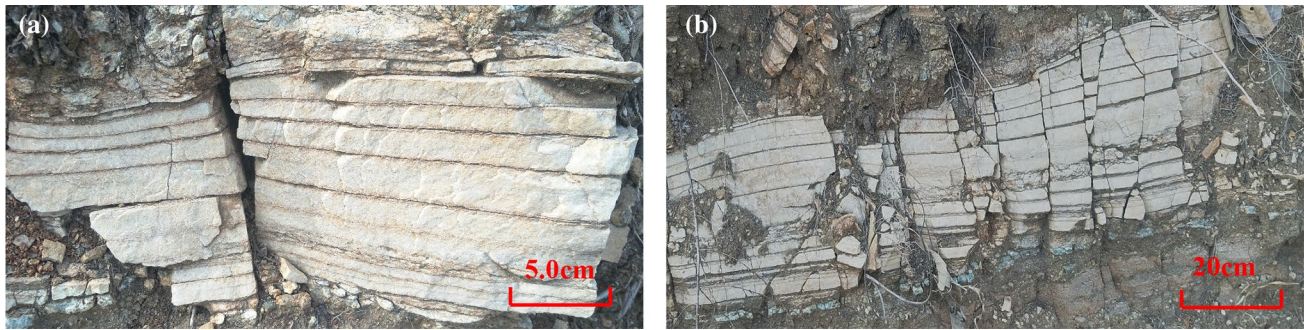


Fig. 1 Natural fracture forms. **a** Cemented natural fractures; **b** natural fracture networks

inconvenient [18]. The discrete element method (DEM) is a meshless numerical tool. By establishing different contact models between particles [19], the hydraulic fracturing processes can be realized. But the DEM method has many mesoscopic parameters which need to be calibrated before modeling and cannot be applied directly to the actual engineering. The newly developed numerical methods such as numerical manifold method (NMM) [20], peridynamics (PD) [21] and material point method (MPM) [22] all have their unique advantages in modeling the interactions of HF and NF, but still have many limitations.

In our work, by improving the traditional SPH method, a set of novel numerical analysis framework aimed at modeling the rock hydraulic fracturing has been proposed, which is called the 2P-IKSPH method (two phases–improved kernel of smoothed particle hydrodynamics). The water–solid particle interaction modes, the automatic conversion algorithm of water particle and damaged particle, the ‘Particle Domain Searching Method’ and the ‘water particle discrimination algorithm’ have all been put forward to realize the simulations of hydraulic fracturing. One typical numerical example of the interactions between HF and NF under different conditions is carried out, the crack propagation processes and the characteristic loads are obtained. The research results can provide some references for the understandings of laws on the hydraulic fracturing and the interaction mechanisms between HF and NF.

2 Concepts of 2P-IKSPH

2.1 Governing Equations

Every particle in 2P-IKSPH method needs to follow four equations, namely (1) continuity equation; (2) momentum equation; (3) energy equation and (4) motion equation, which can be written as:

$$\begin{cases} \frac{d\rho_i}{dt} = \sum_{j=1}^N m_j v_{ij}^\beta \frac{\partial W_{ij,\beta}}{\partial x_i^\beta} \\ \frac{dv_i^\alpha}{dt} = \sum_{j=1}^N m_j \left(\frac{\sigma_i^{\alpha\beta}}{\rho_i^2} + \frac{\sigma_j^{\alpha\beta}}{\rho_j^2} + T_{ij} \right) \frac{\partial W_{ij,\beta}}{\partial x_i^\beta} \\ \frac{de_i}{dt} = \frac{1}{2} \sum_{j=1}^N m_j \left(\frac{\sigma_i^{\alpha\beta}}{\rho_i^2} + \frac{\sigma_j^{\alpha\beta}}{\rho_j^2} + T_{ij} \right) v_{ij}^\beta \frac{\partial W_{ij,\beta}}{\partial x_i^\beta} \\ \frac{dx_i^\alpha}{dt} = v_i^\alpha \end{cases} \quad (1)$$

where ρ is the density of the base particle, t is the calculation time step, m is the mass of the base particle, v is the velocity of the base particle, x is the position of the base particle, $\sigma^{\alpha\beta}$ is the total stress tensor of the base particle, e is the energy of the base particle, $\tau^{\alpha\beta}$ is the shear stress tensor of the base particle, $\varepsilon^{\alpha\beta}$ is the strain tensor of the base particle, T is the artificial viscous part, which can reduce nonphysical oscillations during calculation, and W is the kernel function of the IKSPH method.

2.2 Elastic Solid Equations

The total stress tensor $\sigma^{\alpha\beta}$ consists of hydrostatic pressure p and shear stress τ , which can be expressed as:

$$\sigma^{\alpha\beta} = -p\delta^{\alpha\beta} + \tau^{\alpha\beta} \quad (2)$$

where δ is the Kronecker symbol. The hydrostatic pressure p can be obtained from the equation of state [23]:

$$p = \left(1 - \frac{1}{2}\Gamma\eta \right) p_H + \Gamma\rho e \quad (3)$$

where p_H is the Hugoniot curve function and the Γ is the Gruneisen parameter [24, 25].

In the solid equation, stress is a function of strain and strain rate. By introducing Jaumann ratio [24, 25], the stress rate can be expressed as follows:

$$\dot{\tau}_{\alpha\beta} = B \left(\varepsilon^{\alpha\beta} - \frac{1}{3}\delta^{\alpha\beta}\varepsilon^{\gamma\gamma} \right) + \tau^{\alpha\gamma} R^{\beta\gamma} + \tau^{\gamma\beta} R^{\alpha\gamma} \quad (4)$$

where $\hat{\tau}$ is the stress rate tensor, B is the shear modulus, R is the torsion tensor, which can be written as:

$$R^{\alpha\beta} = \frac{1}{2} \left(\frac{\partial v^\alpha}{\partial x^\beta} - \frac{\partial v^\beta}{\partial x^\alpha} \right) \tag{5}$$

3 Damage Equations of Water-Stress Coupling

3.1 Water–Solid Particle Interaction

The solid–water particle interaction exists between the water particle and their adjacent solid particles. If the the solid particle is adjacent to the water particle, the normal vector between the water particle and the solid particle is then calculated, as shown in Fig. 2, and can be expressed as follows:

$$n_{ij} = (x_{ij}, y_{ij}) / |r_{ij}| \tag{6}$$

where $x_{ij} = x_j - x_i$; $y_{ij} = y_j - y_i$; $r_{ij} = \sqrt{x_{ij}^2 + y_{ij}^2}$. The direction cosine $n_{x,i}$ and $n_{y,i}$ can then be then obtained:

$$n_{x,i} = x_{ij} / |r_{ij}| \tag{7}$$

$$n_{y,i} = y_{ij} / |r_{ij}| \tag{8}$$

The water pressure p_l is assigned to each water particle, then we can calculate the corresponding water pressure component of water particles to solid particles:

$$\begin{cases} \sigma p_{xx} = p_l \cdot n_{x,i}^2 \\ \sigma p_{yy} = p_l \cdot n_{y,i}^2 \\ \sigma p_{xy} = p_l \cdot n_{x,i} \cdot n_{y,i} \end{cases} \tag{9}$$

3.2 Fracture criteria and numerical treatments

The Mohr–Coulomb criterion with a tension cutoff is selected as the fracture criterion, and the formula can be expressed as follows:

$$\sigma_f = \sigma_t \tag{10}$$

$$\tau_f = c + \sigma_f \tan \phi \tag{11}$$

where σ_f and τ_f are the maximum tensile stress and shear stress; σ_t is the tensile strength of the particle; c is the cohesion of the particle; ϕ is the internal friction angle of the particle.

As can be seen from Eq. (1), the derivative of kernel function in traditional SPH method controls the parameter transfer between different particles. Hence, the fracture mark ξ is introduced here (Figs. 3, 4). If the stress components satisfy Eqs. (10) or (11), then the particle is considered to be damaged, and the fracture mark ξ is set to be 0; otherwise, ξ is

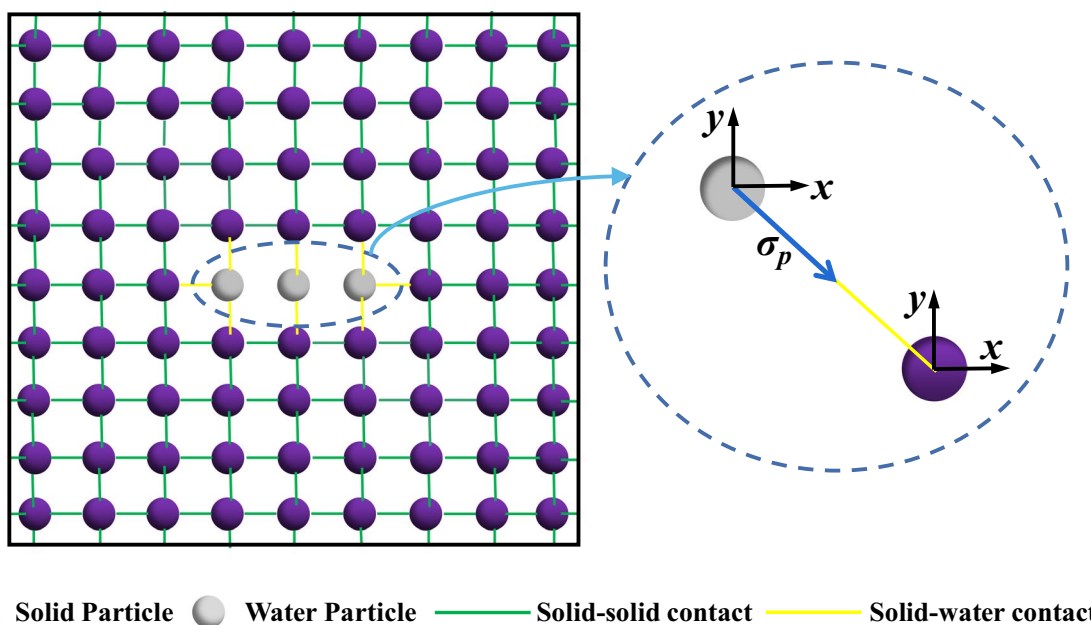


Fig. 2 Water–solid particle interaction

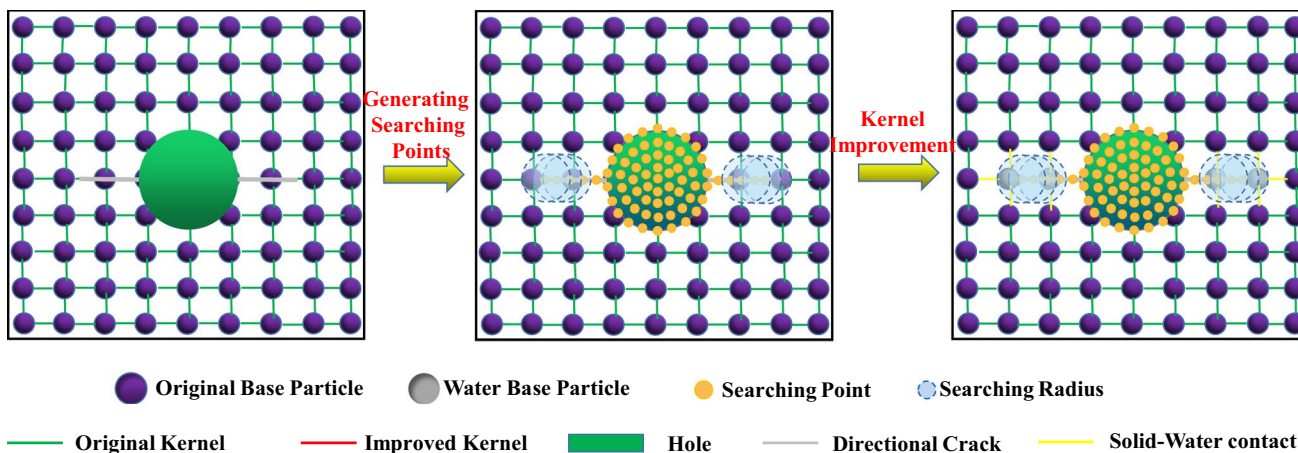


Fig. 3 The particle domain searching method

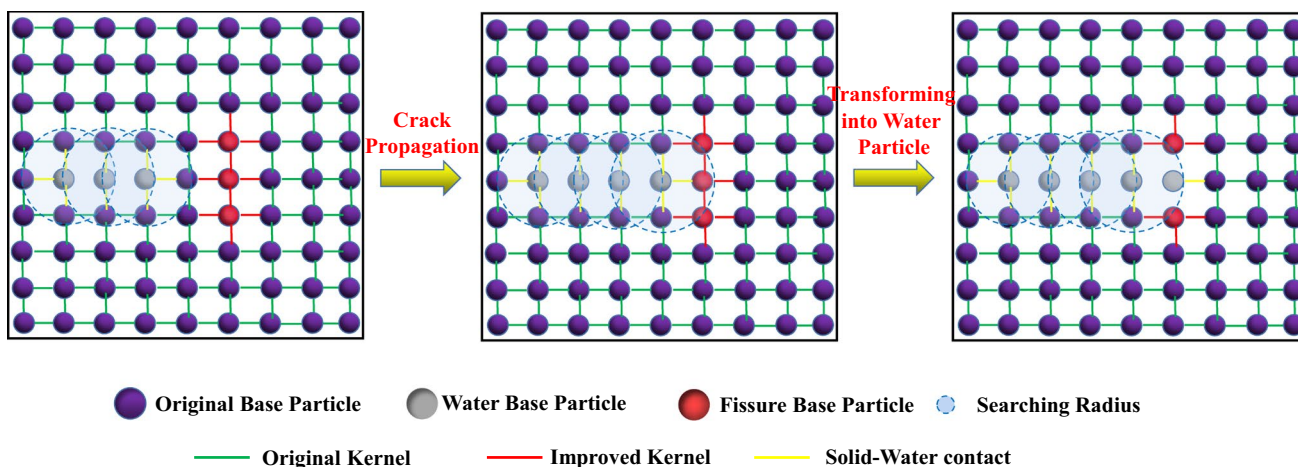


Fig. 4 Water particle discrimination algorithm

set to be 1. Therefore, the improved form of the derivative of kernel function in the 2P-IKSPH method can be written as:

$$\frac{\partial D_{ij,\beta}}{\partial x_i^\beta} = \xi_i \cdot \frac{\partial W_{ij,\beta}}{\partial x_i^\beta} \tag{12}$$

Therefore, the improved governing equation can be expressed as follows:

$$\begin{cases} \frac{d\rho_i}{dt} = \sum_{j=1}^N m_j v_{ij}^\beta \frac{\partial D_{ij,\beta}}{\partial x_i^\beta} \\ \frac{dv_i^\alpha}{dt} = \sum_{j \in S} m_j \left(\frac{\sigma_i^{\alpha\beta}}{\rho_i^2} + \frac{\sigma_j^{\alpha\beta}}{\rho_j^2} + T_{ij} \right) \frac{\partial D_{ij,\beta}}{\partial x_i^\beta} + \sum_{j \in W} m_j \left(\frac{\sigma_i^{\alpha\beta}}{\rho_i^2} + \frac{\sigma_j^{\alpha\beta}}{\rho_j^2} + T_{ij} \right) \frac{\partial D_{ij,\beta}}{\partial x_i^\beta} + \\ \frac{de_i}{dt} = \frac{1}{2} \left(\sum_{j \in S} m_j \left(\frac{\sigma_i^{\alpha\beta}}{\rho_i^2} + \frac{\sigma_j^{\alpha\beta}}{\rho_j^2} + T_{ij} \right) v_{ij}^\beta \frac{\partial D_{ij,\beta}}{\partial x_i^\beta} + \sum_{j \in W} m_j \left(\frac{\sigma_i^{\alpha\beta}}{\rho_i^2} + \frac{\sigma_j^{\alpha\beta}}{\rho_j^2} + T_{ij} \right) v_{ij}^\beta \frac{\partial D_{ij,\beta}}{\partial x_i^\beta} \right) \\ \frac{dx_i^\alpha}{dt} = v_i^\alpha \end{cases} \tag{13}$$

4 Detailed Treatments in 2P-IKSPH

4.1 Particle Domain Searching Method

During the simulation of hydraulic fracturing, the injection well, the hydraulic fractures and the natural fractures need to be generated separately. In this section, the ‘Particle Domain Searching Method’ has been proposed here, which can be expressed as follows:

1. Firstly, different parts such as the injection well, the hydraulic fractures and the natural fractures are geometrically located. The injection well is marked as C_1 , which can be determined by the central coordinate (x_1, y_1) and its radius r_1 . The two hydraulic fractures are marked as l_1 and l_2 separately, which are determined by two endpoints, $l_1: (x_{21}, y_{21}), (x_{22}, y_{22})$ and $l_2: (x_{31}, y_{31}), (x_{32}, y_{32})$.
2. Secondly, a series of searching points are generated on the injecting well C_1 , hydraulic fractures l_1 and l_2 , which are marked as $m_i (i=1,2,\dots,n)$. What should be pointed out is that these searching points should be distributed uniformly on l_1, l_2 , and C_1 ; meanwhile, the average spacing between the searching points should be less than that of real particles.
3. Finally, for each searching point, a searching radius d is assigned. If the real particle is covered by the radius d , then the real particle is transformed into water particle, on which the water pressure p_l is acted on.

4.2 Water Particle Discrimination Algorithm

During the processes of hydraulic fracturing, the water pressure p_l only acts on the HF before the HF approaching NF, and there is no water pressure acting on the NF. When the HF passes through the NF, water media in the HF flow into the NF, and the NF, therefore, transforms into HF. Hence, it is necessary to distinguish the damaged particles (without internal water pressure) from the water particles (with internal water pressure acting on them) in order to correctly apply the internal hydraulic load. In this section, the ‘Water Particle Discrimination Algorithm’ has been proposed, and the details are as follows:

1. Define all the water particles as $W_i (i=1,2,\dots,n)$, and all the damaged particles as $F_i (i=1,2,\dots,n)$.
2. During each calculation circle, the particles that reach the fracture criterion are incorporated into W_i ; meanwhile, the searching circle is generated with the center coordinate of each water particle as the center and the 2 times of the average spacing of the solid particle as the radius.
3. For those damaged particles inside the radius of the searching circle, they are moved to W_i , and water pressure p_l is then activated.

5 Calculation Flowchart of 2P-IKSPH

To summarize, the calculation flowchart can be expressed as follows, which is also shown in Fig. 5.

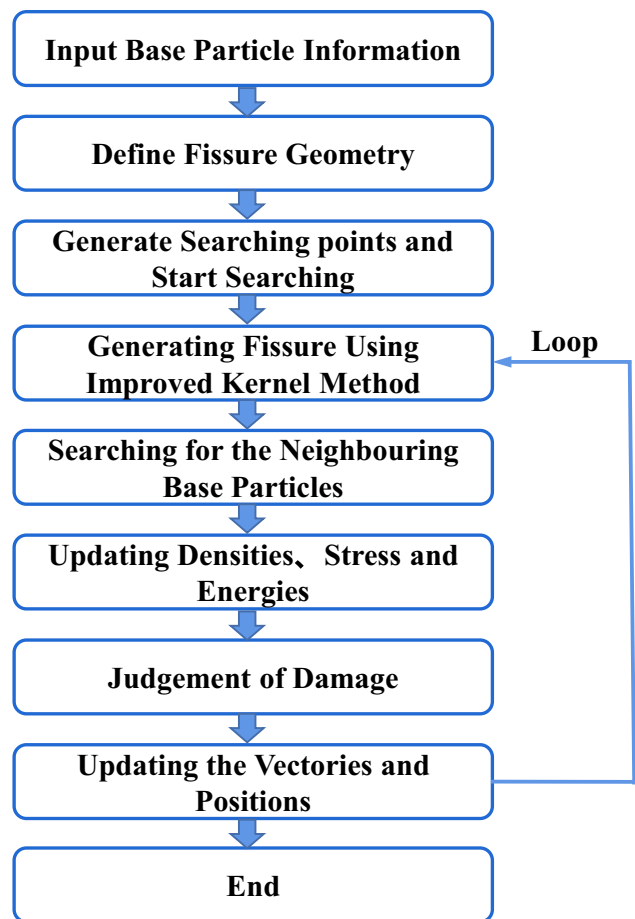


Fig. 5 The flowchart of 2P-IKSPH

1. Input particle basic information, including the coordinates, initial velocities, initial stress, boundary conditions, etc.
2. Define the HF and NF locations, including the coordinates of the endpoints.
3. The searching of water and fissure particle is carried out according to the method in Sect. 4.
4. The particle searching is performed at each time step (the linked list searching algorithm is applied here in this paper), and the smoothing kernel function of each base particle pair is then updated.
5. The density, stress and energy are updated according to the Eq. (13).
6. The fracture state of each base particle is judged according to Eqs. (10) and (11).
7. The velocity and position of each base particle are updated; if the program is not finished, then returns to 3.

6 Numerical Models

6.1 Verification of the Proposed Numerical Simulation Method

To verify the proposed numerical method, the numerical model of a cubic shape with one single crack is established. The model size is $1\text{ m} \times 1\text{ m}$, and one hydraulic fracture with a length of 1 m is prefabricated in the center, on which the internal water pressure 1 MPa is acted on. The confining pressure of 1 MPa is acted on the model side. Figure 6 shows the maximum principal stress distribution of the model calculated by the 2P-IKSPH method proposed in this paper and

the Abaqus software. As can be seen, the calculation results by 2P-IKSPH and Abaqus are consistent, which indicates that the proposed method is accurate and reasonable.

6.2 Numerical Model Details

One typical hydraulic fracturing model with HF and NF is selected for analysis, as shown in Fig. 7. The model size is $1\text{ m} \times 1\text{ m}$. In the center of the model are one injection well and two hydraulic fractures, and two natural fractures are set on both sides. The inclination angle between natural fracture and horizontal direction is θ . The whole model is divided into $300 \times 300 = 90,000$ particles.

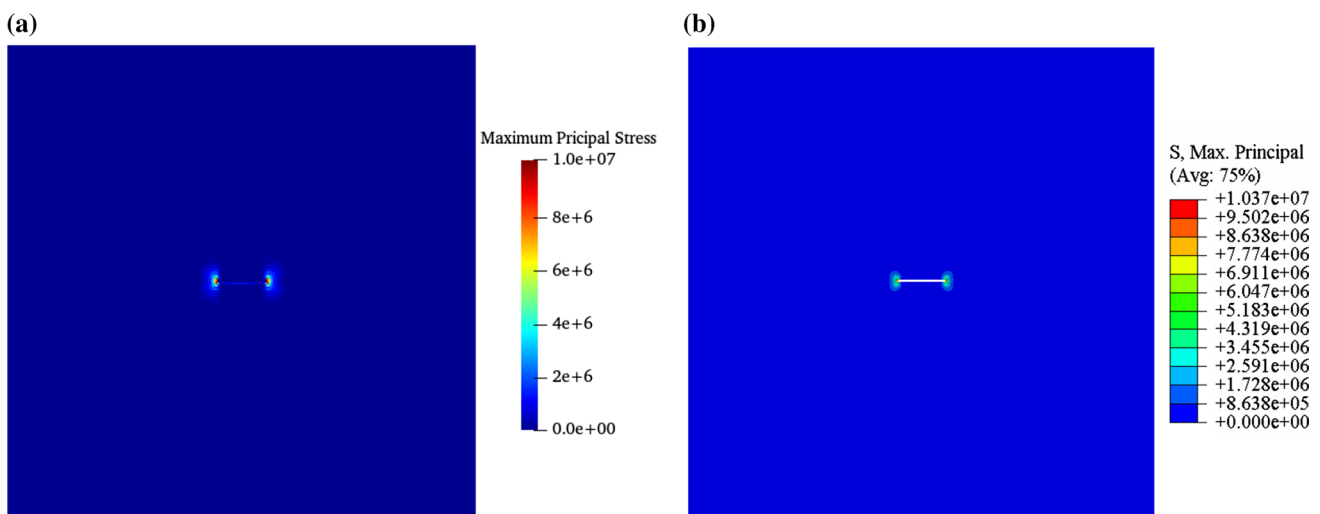


Fig. 6 The maximum principal stress distribution of 2P-IKSPH and Abaqus. **a** Results of 2P-IKSPH; **b** results of Abaqus

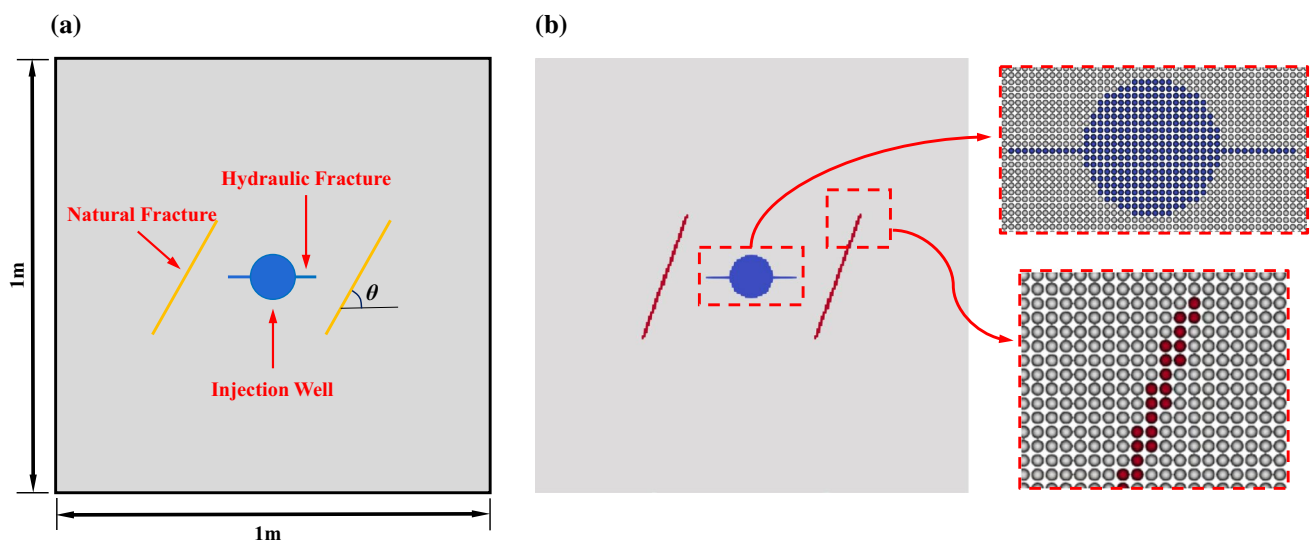


Fig. 7 Numerical model and particle division. **a** Model size; **b** particle divisions and details

In order to investigate the interaction mechanisms between HF and NF under different conditions, the calculation circumstances are set as follows: A: Different confining pressure; B: Different NF inclination angles; C: Different internal water pressure injecting rates. The HF initiation pressure, the approaching pressure and the NF initiation pressure are calculated for each condition. Meanwhile, the interaction modes of HF and NF are also exhibited. The calculation conditions are shown in Table 1.

The calculation parameters are set according to [26]: Elasticity modulus $E=17\text{GPa}$; Poisson’s ratio $\mu=0.14$; cohesive strength $c=25\text{MPa}$; internal friction angle $\varphi=45^\circ$; tensile strength $\sigma_t=25.5\text{MPa}$. Firstly, the in situ stress balance of 3000 steps is carried out, when the boundary stress reaches the predetermined stress, then the internal water pressure is added to the injection well and the hydraulic fracture.

7 Numerical Results

In this section, three characteristic loads are defined for analysis: The HF initiation pressure, which means the initiation internal water pressure of HF; the approaching pressure, which means the internal water pressure when the HF approaches the NF; the NF initiation pressure, which means the initiation internal water pressure of NF. The interaction

modes of HF and NF are also exhibited in the following sections.

7.1 Interaction Between HF and NF Under Different Confining Pressure

Figure 8 shows the interaction modes between HF and NF under different confining pressure. As can be seen, the interaction modes vary under different confining pressures. For those circumstances when the vertical confining pressure is relatively high (condition A1 and A2), crack initiates at the four crack tips of NF; meanwhile, due to the high pressure and the randomness of crack propagation direction, hydraulic fractures are prone to branch in this case, which can increase the hydraulic fracturing area and shale gas production. For the condition when the vertical confining pressure is lower (condition A3), although crack still initiates from the four crack tips of NF, there is no branching cracks occur during hydraulic fracturing compared with condition A1 and A2. For the condition with much lower vertical confining pressure (condition A4), crack initiates on one tip of NF closer to the horizontal boundary, and no branching crack occurs.

Figure 9 shows the characteristic loads under different confining pressure. As can be seen, the characteristic loads decrease with the decrease in vertical confining pressure

Table 1 Calculation conditions

Schematic diagram	Number	Details	Schematic diagram	Number	Details
	A1	$\sigma_x=4\text{MPa}$ $\sigma_y=4\text{MPa}$		B1	$\theta=30^\circ$
	A2	$\sigma_x=4\text{MPa}$ $\sigma_y=3\text{MPa}$		B2	$\theta=50^\circ$
	A3	$\sigma_x=4\text{MPa}$ $\sigma_y=2\text{MPa}$		B3	$\theta=70^\circ$
	A4	$\sigma_x=4\text{MPa}$ $\sigma_y=1\text{MPa}$		B4	$\theta=90^\circ$
	C1	$v=100\text{Pa/Step}$			
	C2	$v=400\text{Pa/Step}$			
	C3	$v=700\text{Pa/Step}$			
	C4	$v=1000\text{Pa/Step}$			

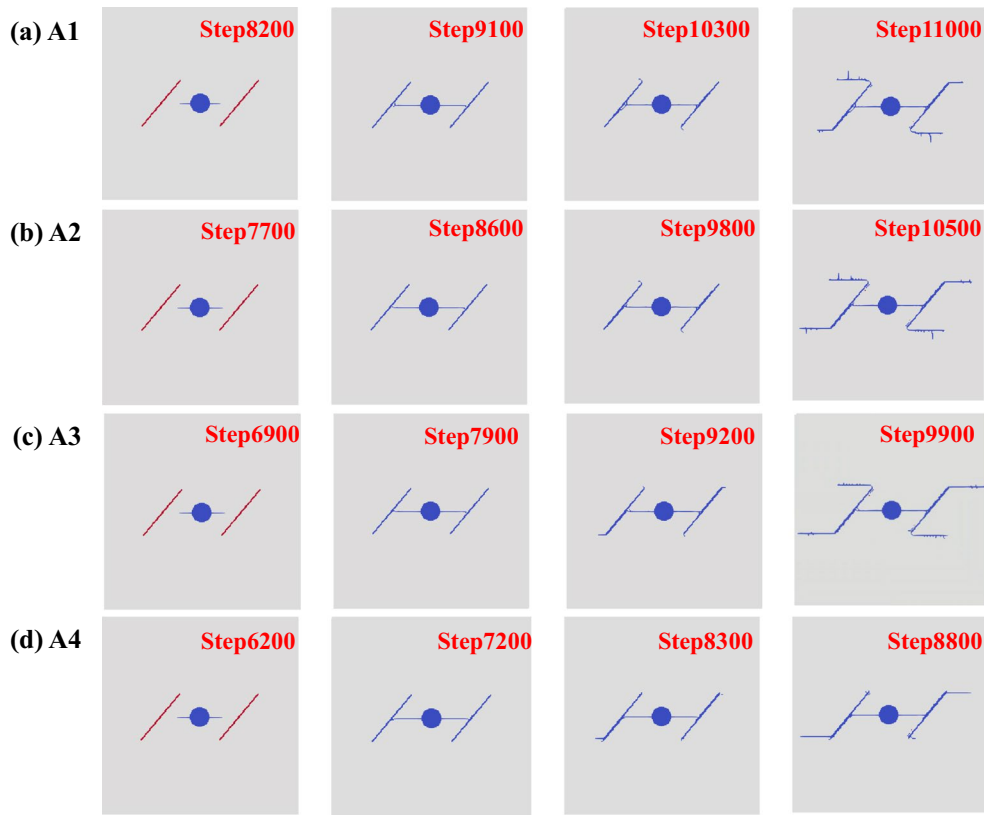


Fig. 8 Interactions between HF and NF under different confining pressure

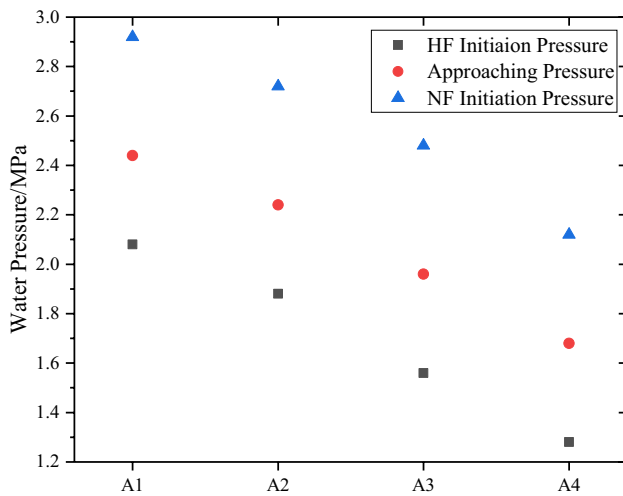


Fig. 9 Characteristic loads under different confining pressure

σ_y , which means that the HF and NF are more easily to initiate and propagate in this situation.

7.2 Interaction Between HF and NF Under Different NF Inclination Angles

Figure 10 shows the interaction modes under different NF inclination angles. As can be seen, for the condition with small inclination angles (B1, $\theta = 30^\circ$), the crack initiation not only occurs on the HF tips, but also on the vertical side of injection well, which indicates that the NF will influence the hydraulic fracturing process when NF is near the injection well. Meanwhile, when HF approaches NF, the branching cracks occur, which means that the small inclination angles will lead to nonuniform expansions of NF. For the condition when the inclination angle is 50° (B2), the crack initiation occurs only at the four crack tips of NF, but NF branches after propagating to a certain extent. For the condition with large inclination angles (B3, $\theta = 70^\circ$; B4, $\theta = 90^\circ$), the crack initiates at NF tips, and no branching crack occurs.

Figure 11 shows the characteristic loads under different NF inclination angles. As can be seen, the HF initiation pressure first increases then decreases with the increase in NF inclination angles, and reaches the maximum when the inclination angle is 50° (B2), while the approaching pressure and the NF initiation pressure show a decreasing trend.

Fig. 10 Interactions between HF and NF under different NF inclination angles

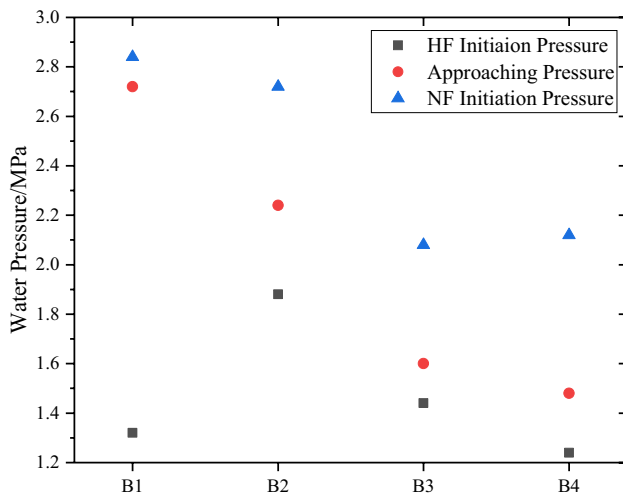
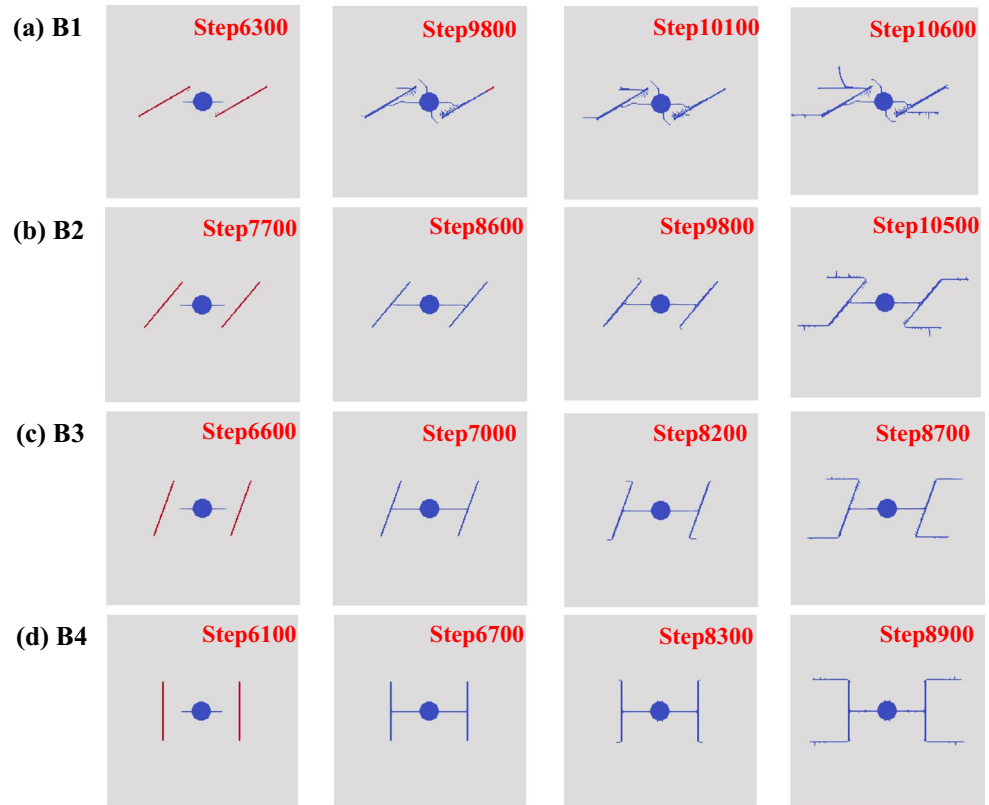


Fig. 11 Characteristic loads under different NF inclination angles

7.3 Interaction Between HF and NF Under Different Injecting Rates

Figure 12 shows the interaction modes under different internal water pressure injecting rates. As can be seen, when the injection rates are relatively low (C1, $v = 100$ Pa/Step), crack initiates only on the one tip of NF closer to the horizontal boundary. However, when the injection rate is larger (C2,

C3, C4), crack initiates at the four tips of NF, and branching crack occurs, which means that increasing the injection rate will increase the hydraulic fracturing area.

Figure 13 shows the characteristic loads under different internal water pressure injection rates. As can be seen, the characteristic loads show a trend of firstly increasing then decreasing with the increase in injection rates. What should be noticed is that when the injection rates are relatively lower (C1, $v = 100$ Pa/Step), the characteristic loads are much smaller, but when the injection rate is larger ($v \geq 400$ Pa/Step), the approaching pressure and the NF initiation pressure increase dramatically, which means that NF is hard to initiate and propagate under high injection rates.

8 Discussions

8.1 Rationality of Numerical Simulation

Figure 14 shows the typical interaction modes between HF and NF [26]: (1) Arresting, which means the HF is arrested by NF; (2) crossing, which means the HF propagates through the NF; (3) dilation, which means that NF expands due to the internal water pressure; (4) activation, which means the crack initiates at NF tips; (5) offset, which means crack initiates in the middle of NF. The interaction modes of HF and NF in our simulation are included in Fig. 14, which can

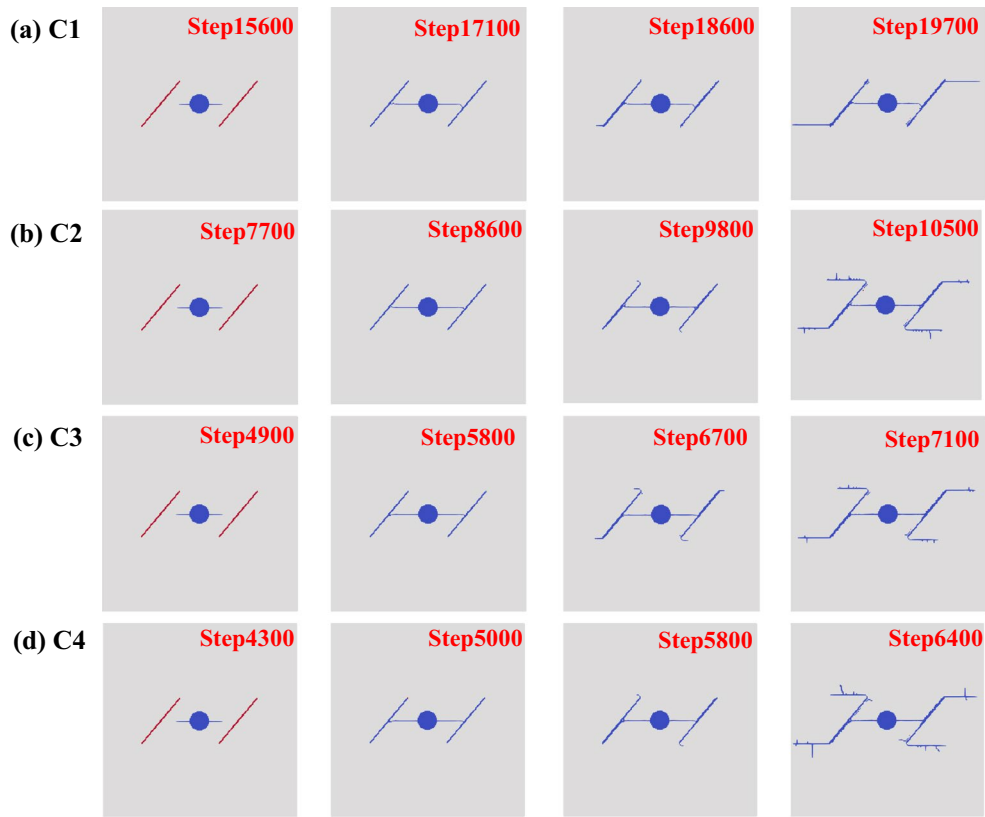


Fig. 12 Interactions between HF and NF under different injection rates

verify the rationality of 2P-IKSPH. However, as can be seen from Figs. 8, 10, 12, only arresting, arresting + dilation and activation are observed, which may be related to the specified calculation conditions and boundary conditions in this paper.

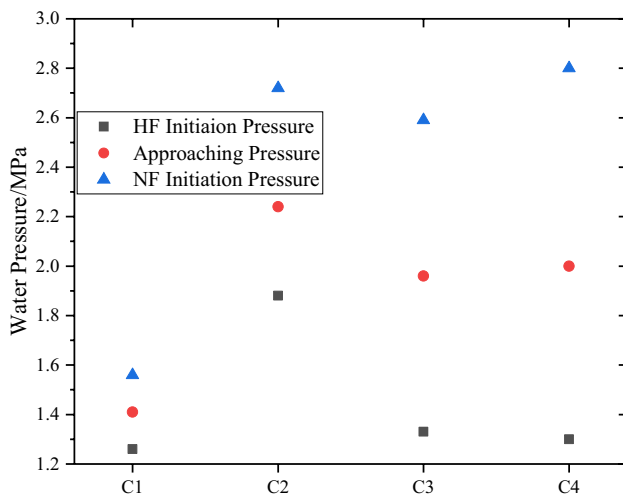


Fig. 13 Characteristic loads under different injection rates

In our paper, the interaction modes under different conditions are systematically simulated. Apart from the traditional interaction modes, the activated NF branches under high vertical confining pressure, low NF inclination angles and high injection rates. Figure 15 shows the branching phenomenon in [27] (Fig. 15(a)) and their simulation results [27] (Fig. 15(b)). We can see that the simulation results by 2P-IKSPH are more natural, independent of the grid, and can truly reflect the branching laws of NF, which is also the advantage of the proposed 2P-IKSPH.

8.2 Application Prospects of 2P-IKSPH in Numerical Simulation of Shale Gas Hydraulic Fracturing

In this paper, by improving the smoothing kernel function in the traditional SPH method, the brittle fracture characteristics of particles in the mesoscale are realized. At the same time, the interaction algorithm of solid–water particle and the automatic transformation algorithm from damage particles to water particles are proposed to realize the hydraulic fracturing process. The ‘particle domain searching method’ and ‘water particle discrimination algorithm’ have been put forward to realize the simulation of complex interactions between HF and NF. Compared with traditional FEM, the 2P-IKSPH method proposed in this paper does not

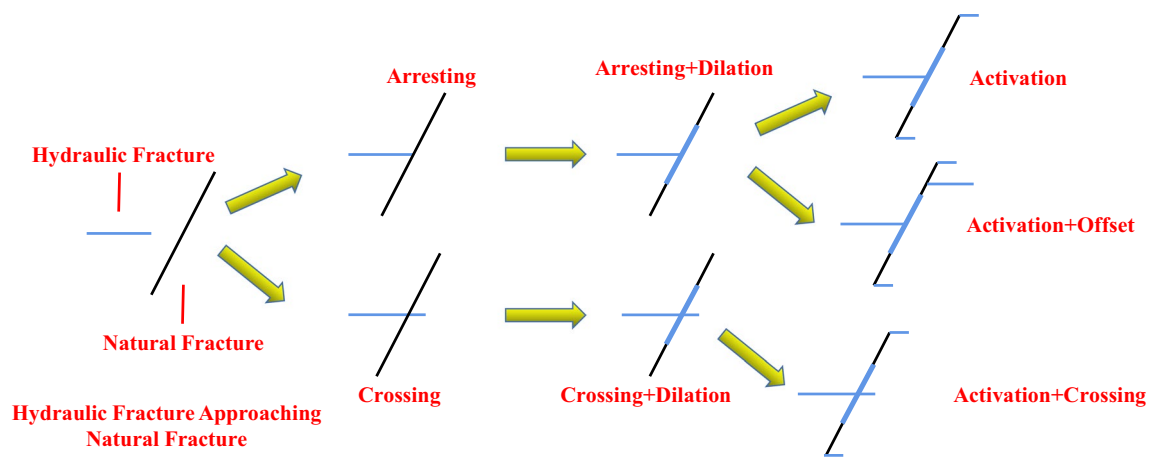


Fig. 14 Typical interaction modes of HF and NF [26]

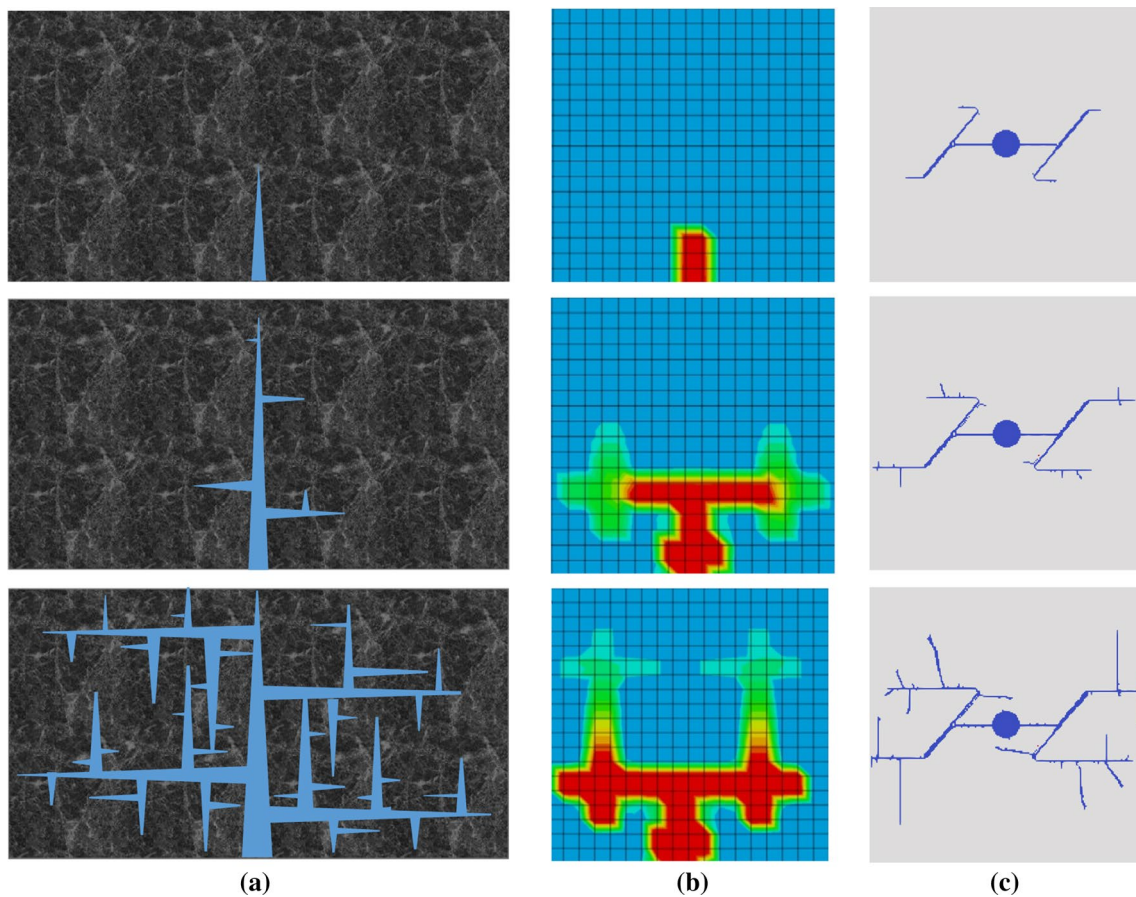


Fig. 15 NF branching phenomenon. **a** Schematic illustration of crack branching caused by NF [27]; **b** numerical simulation of NF branching in [27]; **c** numerical simulation of NF branching by 2P-IKSPH

depend on the grids and does not need to re-divide mesh grids during calculation. Meanwhile, it is suitable for dealing with problems of large deformation and discontinuity, and the interaction process between HF and NF as well as the branching characteristics of NF can be dynamically

reflected. Therefore, applications of 2P-IKSPH in the simulation of hydraulic fracturing of shale gas are promising.

It should be pointed out that the size of the numerical model in this paper is small scale, and the boundary conditions are artificially formulated, which is different from

the actual engineering conditions. However, the calculation conditions selected in this paper are representative, which can reflect the typical interaction modes between HF and NF to a certain extent, and the engineering practice can also be simulated by 2P-IKSPH. What should be noticed is that engineering practical problems are mostly 3D problems, and the simplified 2D model cannot fully represent 3D. At the same time, the computational efficiency of 3D numerical model is relatively low. So, developing high performance 3D 2P-IKSPH program will be the future research direction.

9 Conclusions

1. Based on the traditional SPH method, a new numerical method named 2P-IKSPH has been proposed, which can realize the simulations of hydraulic fracturing.
2. The ‘Particle Domain Searching Method’ and the ‘water particle discrimination algorithm’ have been proposed to realize the complex interactions between HF and NF.
3. The interaction modes of HF and NF include arresting, arresting + dilation, activation and branching, and there are great differences in the characteristic loads under different conditions.
4. 2P-IKSPH method has great potential in the numerical simulations of hydraulic fracturing, and developing high performance 3D 2P-IKSPH program will be the future research directions.

Acknowledgements We acknowledge the financial supports of the National Natural Science Fund (Grant No. U1765204), the National Natural Science Found (51409170) and “the Fundamental Research Funds for the Central Universities”. Meanwhile, the authors greatly wish to express their thanks to Professor Bi Jing, Wuwen Yao, and Yongchuan Yu for their technical supports in the IKSPH programing.

References

1. Jiang, Y.; Lian, H.; Nguyen, V.P.; et al.: Propagation behavior of hydraulic fracture across the coal-rock interface under different interfacial friction coefficients and a new prediction model. *J. Nat. Gas Sci. Eng.* **68**, 102894 (2019)
2. Chen, Z.; Yang, Z.; Wang, M.: Hydro-mechanical coupled mechanisms of hydraulic fracture propagation in rocks with cemented natural fractures. *J. Pet. Sci. Eng.* **163**, 421–434 (2018)
3. Dontsov, E.V.: Propagation regimes of buoyancy-driven hydraulic fractures with solidification. *J. Fluid Mech.* **797**, 1–28 (2016)
4. Cappa, F.; Guglielmi, Y.; Merrien Soukatchoff, V.; et al.: Evaluation of coupled hydromechanical analysis of a fractured rock mass by the multi-scale comparison between experimental and numerical modeling datas from the coaraze natural site. *Langmuir* **19**(17), 6987–6993 (2014)
5. Clark, J.B.: A hydraulic process for increasing the productivity of wells. *J. Pet. Technol.* **1**(1), 1–8 (1949)

6. Wang, Q.; Chen, X.; Jha, A.N.; Rogers, H.: Natural gas from shale formation e the evolution, evidences and challenges of shale gas revolution in United States. *Renew. Sustain. Energy Rev.* **30**, 1–28 (2014)
7. Less, C.; Andersen, N.: Hydrofracture: state of the art in South Africa. *Appl. Hydrogeol.* **2**(2), 59–63 (1994)
8. Aitssi, L.; Villeneuve, J.; Rouleau, A.: Utilization of a stochastic model of fractured rock for the study of the hydraulic properties of a fissured mass. *Can. Geotech. J.* **26** (1989)
9. Zheng, Y.; Liu, J.; Lei, Y.: The propagation behavior of hydraulic fracture in rock mass with cemented joints. *Geofluids* **5406870** (2019)
10. Taleghani, A.D.; Gonzalez, M.; Shojaei, A.: Overview of numerical models for interactions between hydraulic fractures and natural fractures: challenges and limitations. *Comput. Geotech.* **71**(1), 361–368 (2016)
11. Zhou, J.; Chen, M.; Jin, Y.: Study on shear failure mechanism of natural fracture in fracturing. *J. Rock Mech. Eng.* **2008**(S1), 2637–2641 (2008)
12. Blanton, T.L.: Propagation of hydraulically and dynamically induced fractures in naturally fractured reservoirs. In: *SPE Unconventional Gas Technology Symposium [S.L.]*: Society of Petroleum Engineers (1986)
13. Zhang, S.; Guo, T.; Zhou, T.: Mechanism of fracture expansion in natural shale fracturing. *J. Pet.* **35**(03), 496–503+518 (2014)
14. Li, Y.; Xu, W.; Zhao, J.: Criteria for determining hydraulic fractures passing through natural fractures in shale reservoirs. *Gas Ind.* **35**(07), 49–54 (2015)
15. Liu, Y.; Ai, C.: Study on the law of natural fracture opening multistage fracturing induced stress. *Oil Drill. Technol.* **43**(01), 20–26 (2015)
16. Li, Y.; Wang, Y.; Zhao, J.: Calculation model of fracturing angle of shale reservoir considering multiple seam stress interference. *Nat. Gas Geosci.* **26**(10), 1979–1983+1998 (2015)
17. Tang, C.; Li, L.; Li, C.: Analysis of geotechnical engineering stability RFP strength reduction. *J. Rock Mech. Eng.* **2006**(08), 1522–1530 (2006)
18. Branco, R.; Antunes, F.V.; Costa, J.D.: A review on 3D-FE adaptive remeshing techniques for crack growth modelling. *Eng. Fract. Mech.* **141**, 170–195 (2015)
19. Zhang, L.: Systematic investigation of the planar shape of rock fractures using PFC3D numerical experiments. *Can. J. Geol.* **28**(6), 750–757 (2012)
20. Ohnishi, Y.; Sasaki, T.; Koyama, T.; et al.: Recent insights into analytical precision and modelling of DDA and NMM for practical problems. *Geomech. Geoen.* **9**(2), 97–112 (2014)
21. Zhou, X.P.; Shou, Y.D.; Qian, Q.H.: Three-dimensional nonlinear dynamic strength criterion for rock. *Int. J. Geomech.* **16**(2), 04015041 (2016)
22. Müller, A.; Vargas, E.A.: Stability analysis of a slope under impact of a rock block using the generalized interpolation material point method (GIMP). *Landslides* **16**, 751–764 (2019)
23. Vonneumann, J.; Richtmyer, R.D.: A Method for the numerical calculation of hydrodynamic shocks. *J. Appl. Phys.* **21**(3), 232–237 (1950)
24. Liu, G.R.; Liu, M.B.: *Smoothed particle hydrodynamics: a mesh-free particle method*. World Scientific Press (2003)
25. Libersky, L.D.; Petschek, A.G.; Carney, T.C.; et al.: High strain Lagrangian hydrodynamics: a three-dimensional SPH code for dynamic material response. *J. Comput. Phys.* **109**(1), 67–75 (1993)
26. Janiszewski, M.; Shen, B.; Rinne, M.: Simulation of the interactions between hydraulic and natural fractures using a fracture mechanics approach. *J. Rock Mech. Geotech. Eng.* **11**(6), 1138–1150 (2019)
27. Rahimi-Aghdam, S.; Chau, V.T.; Lee, H.; et al.: Branching of hydraulic cracks enabling permeability of gas or oil shale with closed natural fractures. *Proc. Natl. Acad. Sci.* **116**, 1532–1537 (2019)

